Eur. Phys. J. D **28**, 199–209 (2004)
DOI: 10.1140/epjd/e2003-00313-4

THE EUROPEAN PHYSICAL JOURNAL D

High precision description of the rovibronic structure of the I_2 B-X spectrum*

H. Knöckel[a], B. Bodermann[b], and E. Tiemann

Institut für Quantenoptik, Universität Hannover, Welfengarten 1, 30167 Hannover, Germany

Received 27 May 2003 / Received in final form 9 October 2003
Published online 23 December 2003 –

Abstract. A precise description of the B-X spectrum of the I_2 molecule has been developed. All presently available high precision measurements on the B-X spectrum of the I_2 molecule in the visible were introduced into a model based on molecular potentials for the two electronic states involved, the transition frequencies being the differences of the energy eigenvalues for the rovibrational levels in those potentials. This approach allows, depending on the quality of the input data, a prediction of iodine lines with a 2σ uncertainty of less than 30 MHz from 514 nm to 815 nm of most bands in that range. In the range between 526 nm to 667 nm, where highly precise systematic measurements exist, a smaller 2σ uncertainty of 3 MHz is achieved. Moreover, a precise local model description of selected bands of the B-X spectrum has been derived from high precision measurements of iodine lines in the near infrared between 778 nm and 815 nm. This approach by using a Dunham parameter description allows to predict lines of these bands with a 1σ uncertainty of less than 200 kHz. All this information including the systematically studied hyperfine structure can be combined in a computer program for predicting the details of the iodine B-X spectrum with high reliability, serving as a convenient tool in spectroscopic calibration tasks.

PACS. 33.15.Mt Rotation, vibration, and vibration-rotation constants – 33.20.Kf Visible spectra – 34.20.Cf Interatomic potentials and forces

1 Introduction

The iodine spectrum has a good tradition as a frequency reference in the visible and in the NIR. The iodine atlas by Gerstenkorn et al. [1] permits a frequency calibration in the range between 330 THz (11000 cm^{-1}) and 600 THz (20000 cm^{-1}) using Doppler-broadened lines. Doppler-free iodine lines have been used not only as a convenient reference for frequency stabilisation of lasers, but also as frequency references at a high level of accuracy of few parts in 10^{-9} or even much better [2–9]. Some of them are recommended as wavelength standards by the *Comité International des Poids et Mesures* (CIPM) [10]. Most of these lines are spread accidentally in the visible spectrum, given by coincidences with frequencies of the lasers to be stabilized. Recently, quite accurate systematic measurements band by band of iodine lines between 570 nm and 655 nm were published [11–13], and highly precise measurements of iodine lines in the near infrared are available now [14–17]. New lines were reported using diode lasers around 633 nm [18], and also the region around 532 nm has been covered with high precision [19–23]. Furthermore, Kato et al. published an atlas covering the range from 15000 cm^{-1} (667 nm) to 19000 cm^{-1} (526 nm), containing Doppler free spectra of this whole range [24]. In total, the availability of such a large body of data leads to the idea to look for a highly precise model description of the B-X spectrum, allowing the precise reproduction of all reported lines and a prediction of frequencies of unmeasured lines for calibration purposes.

For the case of Doppler broadened lines, already Gerstenkorn et al. showed, that it is possible to describe their data set of transition frequencies of 17800 iodine lines to an uncertainty level of $\delta\nu/\nu \approx 10^{-7}$ using as an adequate description the Dunham series based upon the physical model of a vibrating rotor, and to reduce the data to as few as 46 fitted molecular parameters [25]. Martin et al. determined molecular parameters describing the emission spectrum of iodine in the range between 7400 cm^{-1} and 18350 cm^{-1} to an uncertainty level of several 10^{-7} [26], thereby characterizing the molecular ground state level structure nearly up to the dissociation limit.

The high precision data stem from experiments in which the Doppler broadening was small, and the frequencies refer to resolved hyperfine transitions which underlie

* A supplementary table is only available in electronic form at `http://www.edpsciences.org`

[a] e-mail: `knoeckel@iqo.uni-hannover.de`
[b] *Present address:* Physikalisch-Technische Bundesanstalt, Bundesallee 100, 38116 Braunschweig, Germany.

the Doppler broadened lines observed in a linear absorption experiment. This fact calls for dividing the model approach into two steps.

First the hyperfine splitting has to be removed from the measured frequencies. Thus precise models for the description of the hyperfine structure of the B-X spectrum are required. In a recent paper we introduced models capable of describing the hyperfine structure with a 2σ uncertainty of few 10 kHz [27].

Second the rovibrational level structure has to be described by appropriate models. This is the topic of the present paper.

The paper roughly is organized in two parts. The first one is concerned with our systematic near infrared high precision measurements of absolute frequencies and of frequency differences. Here it is of great advantage to use a "local" description, which is restricted to the range of bands prevailing in the iodine spectrum in the range between 778 nm and 815 nm, but which is able to exploit the high precision of the measurements to yield highly accurate predictions of frequencies.

In the second part a new model approach is presented, which uses all precise data of the B-X system available in the whole visible and near infrared spectral range. The aim is to offer a range as large as currently possible with a prediction uncertainty as small as possible. As it will be shown in the following, an overall description of fairly large parts of the iodine spectrum with a 2σ uncertainty level of less than 3 MHz is possible.

2 Description of the data in the near infrared range from 778 nm to 815 nm

Our measurements in the near infrared cover the wavelength range between 778 nm and 815 nm. Here several lines were calibrated absolutely with uncertainties mostly much smaller than 80 kHz [14,15,17], and also difference frequencies between hyperfine lines of different rotational transitions were determined with uncertainties less than 50 kHz [28]. The experimental details of the absolute calibrations have already been described in those references. For the measurement of difference frequencies the beams of two iodine stabilized lasers, each stabilized to different iodine hyperfine lines of different rovibronic transitions, were overlapped on a fast photodiode and the beat frequencies were counted with a microwave counter for frequencies up to 26 GHz. The counting results were checked in different experimental settings to determine the scatter in the realisation of the laser locks to the transition frequencies. Typical intervals of such scatter were around 10 kHz or less. The measured frequencies include the frequency shift due to the hyperfine interaction. They were subtracted using the interpolation formulae for the hyperfine parameters given in our recent paper [27]. To the derived data set, containing difference frequencies of rotational lines and rovibronic ones of the B-X system, lines of the iodine atlas by Gerstenkorn [1] were added to fill some of the remaining gaps in the quantum number sequence of the bands to check the internal consistency. These data bear much larger uncertainties than the formerly described ones. The accuracy of the frequencies given in the iodine atlas was improved compared to [1] (see discussion in Sect. 3.1) by a line shape analysis.

Only frequencies from the bands $v' = 0 - v'' = 12$, 13, 14, 15, 16, and 17 were used to keep the number of parameters for the description of the upper state as small as possible. A local representation using the usual Dunham ansatz [29] was applied:

$$E_B(v', J') - E_X(v'', J'') = S_e + \sum_{l,k} S^B_{lk} \left(v' + \frac{1}{2}\right)^l [J'(J'+1)]^k - \sum_{l,k} S^X_{lk} \left(v'' + \frac{1}{2}\right)^l [J''(J''+1)]^k, \quad l, k = 0, 1, 2, ... \quad (1)$$

Traditionally, the Dunham parameters are named be Y_{lk}. Here we use S_{lk}, because the parameters have a very limited range of allowed quantum numbers. By this definition we hope to avoid confusion in usage. The number of parameters was reduced as much as possible. So for the upper state B, where only $v' = 0$ is used, the vibronic energy of the band origin was confined to one parameter, here labeled as S_0. Similarly a single parameter S_k for each power k of $J(J+1)$ with k up to $k = 4$ was used:

$$S_0 = S_e + \sum_l S^B_{l0} \left(\frac{1}{2}\right)^l$$
$$S_k = \sum_l S^B_{lk} \left(\frac{1}{2}\right)^l . \quad (2)$$

For the ground state, also as few as possible parameters for the narrow range of levels were selected, in order to describe the data satisfactorily. The standard deviation of the fit is 40 kHz. The resulting parameters are listed in Table 1. The uncertainty limits given correspond to one standard deviation. The number of digits given in the table corresponds to those necessary for a round off smaller than few kHz. The fitted parameters are highly correlated, so that the uncertainties of predicted frequencies cannot be calculated from these parameter uncertainties alone. Based on the covariance matrix of the fit, in Figure 1 we give uncertainty limits for arbitrary frequencies calculated from these parameters for those bands, for which high precision measurements are available. The symbols (circles, triangles, etc.) of each curve in the figure correspond to $\mathrm{R}(J'')$ lines from smaller to greater wavelengths with $J'' = 20$ to 120 in steps of ten, then 150 to 190 in steps of ten and finally 210. The graphs for $\mathrm{P}(J'')$ lines will not show significant differences. Especially for the bands 0-15 and 0-14, which include most of the high precision measurements, the 1σ prediction uncertainty is well below 100 kHz for moderate J values, so such high accuracy can be expected for reference lines of these bands between 778 and 796 nm. Selecting the proper J'' of the other bands,

Table 1. Dunham parameters derived from fit of the near infrared data of bands (v', v'') with $v' = 0$ and $v'' = 12$, ..., 17 and $J'' \leq 242$.

	lower state $X^1\Sigma_g^+$ [cm^{-1}]		upper state $B0_u^+$ [cm^{-1}]
S_{10}	$0.21479058554 \times 10^3 \pm 0.95 \times 10^{-3}$	S_0	$15832.7358035 \pm 0.56 \times 10^{-2}$
S_{20}	$-0.6349014655 \pm 0.45 \times 10^{-4}$	S_1	$0.289260041202 \times 10^{-1} \pm 0.42 \times 10^{-8}$
S_{40}	$-0.31552791 \times 10^{-4} \pm 0.29 \times 10^{-7}$	S_2	$-0.62353693595 \times 10^{-8} \pm 0.60 \times 10^{-12}$
S_{01}	$0.373816471278 \times 10^{-1} \pm 0.16 \times 10^{-6}$	S_3	$-0.22689095 \times 10^{-14} \pm 0.19 \times 10^{-16}$
S_{11}	$-0.1166181096942 \times 10^{-3} \pm 0.28 \times 10^{-7}$	S_4	$-0.4269941 \times 10^{-20} \pm 0.16 \times 10^{-21}$
S_{21}	$-0.996620979 \times 10^{-7} \pm 0.16 \times 10^{-8}$		
S_{31}	$-0.895649619 \times 10^{-8} \pm 0.31 \times 10^{-10}$		
S_{02}	$-0.4608461804 \times 10^{-8} \pm 0.18 \times 10^{-11}$		
S_{12}	$-0.1196947480 \times 10^{-10} \pm 0.24 \times 10^{-12}$		
S_{22}	$-0.9829624898 \times 10^{-12} \pm 0.78 \times 10^{-14}$		
S_{03}	$-0.36003776 \times 10^{-15} \pm 0.22 \times 10^{-16}$		
S_{13}	$-0.33513423 \times 10^{-16} \pm 0.18 \times 10^{-17}$		
S_{04}	$0.6778317 \times 10^{-21} \pm 0.20 \times 10^{-21}$		
S_{14}	$-0.1441870 \times 10^{-21} \pm 0.16 \times 10^{-22}$		

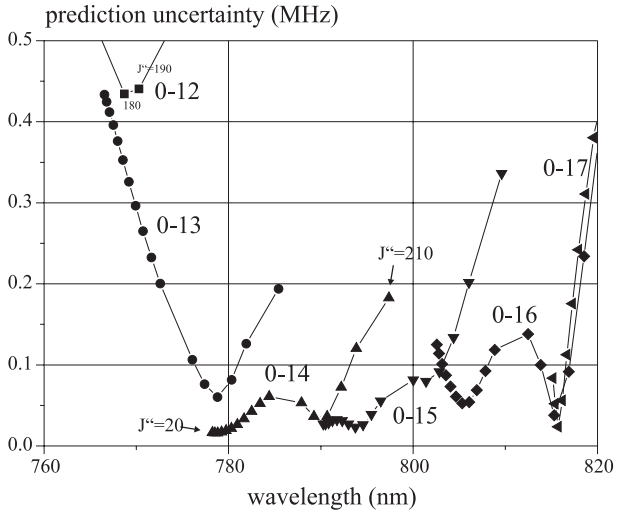

Fig. 1. 1σ prediction uncertainty for R lines of the 0-12 to 0-17 bands in the near infrared. The symbols in each band correspond from left to right to $J'' = 20$, 30, 40, 50, 60, 70, 80, 90, 100, 110, 120, 150, 160, 170, 180, 190, and 210.

lines within the wavelength range from roughly 775 nm to 815 nm can be predicted with 1σ accuracies well below 200 kHz using this local model.

3 Description of the visible and NIR spectrum

3.1 Discussion of the data available

A large number of precisely known transition frequencies is already available in the literature [8–23,30]. A dense grid of lines exists between 560 nm and 650 nm [11–13], with uncertainties of the transition frequencies at a 1 MHz level. This grid also provides systematic information about the molecular bands involved. A narrow range around 532 nm has been determined with very high precision [19–21], containing information of upper vibrational states $32 \leq v' \leq 36$. Some hyperfine resolved transition frequencies in the near infrared were given by Rakowsky [31] at a 30 MHz level of uncertainty. The other precise measurements are distributed fairly irregular in the visible iodine spectrum. These data were supplemented by frequencies derived from the iodine atlas recently published by Kato et al. [24], which covers the spectral range from 526 nm to 667 nm and contains, in addition to the Doppler broadened spectrum, also the Doppler reduced saturation spectrum, together with a calibrated marker spectrum. The authors give an accuracy of better than ± 3 MHz for lines derived from the atlas. For the region from 526 nm to 560 nm, we determined transition frequencies quite systematically from this atlas.

Rong et al. [32] only give difference frequencies between hyperfine components. Quantum numbers were assigned using the iodine atlas [1] and the Dunham parameters of [25]. Then these differences were combined with the wavelength comparison of the R(25) 25-0 line by Grieser et al. [33] (remark: in that paper erroneously an assignment of R(25) 26-0 was given) to give precise absolute frequencies for 16 additional lines of bands 24-0, 25-0, 26-0, 27-1 and 28-1.

All absolute frequencies of hyperfine transitions were corrected for the shift due to the hyperfine interaction, in order to get the frequency of the pure rovibronic transition. If the hyperfine parameters for the transition under consideration were known, these were used to calculate the hyperfine shift, otherwise the hyperfine parameters were interpolated using the formulae published recently [27].

For lines derived from the saturation spectra in Kato's atlas, apart from few exceptions lines of even J were chosen, and the absolute frequencies of the hyperfine components a_1, a_{10} and a_{15} were determined, because these are single lines and unblended and following the

Table 2. Recalibration rules for frequencies from iodine atlas by Gerstenkorn et al. [1].

atlas	frequency correction of wavenumber ν [cm^{-1}]	estimated 1σ uncertainty	[10^{-3}cm^{-1}]
atlas I, part 1 (11000–13000 cm^{-1})	$\nu_{\rm corr} = \nu_{\rm atlas}$	J'' even: 0.65	J'' odd: 1.1
atlas I, part 2-4 (13000–14000 cm^{-1})	$\nu_{\rm corr} = \nu_{\rm atlas} - 2.5 \times 10^{-3}$	J'' even: 1.0	J'' odd: 1.5
atlas II, III, (14000–20000 cm^{-1})	$\nu_{\rm corr} = \nu_{\rm atlas}\ (1 + 1.7 \times 10^{-7}) - 8.1 \times 10^{-3}$	J'' even: 0.71	J'' odd: 0.99

Table 3. Shifts of "pure" rovibronic frequency ν_{rv} with respect to corrected frequency of line maximum $\nu_{\rm corr}$, and profile data.

atlas	frequency shift ν [cm^{-1}]	cell temp °C	FWHM rect. [MHZ]	FWHM sinc [MHZ]
atlas I, part 1	J'' even: $\nu_{rv} = \nu_{\rm corr}$	790	750[1]	750[1]
(11000–13000 cm^{-1})	J'' odd: $\nu_{rv} = \nu_{\rm corr} - 6.3(2.0) \times 10^{-4}$			
atlas I, part 2-4	J'' even: $\nu_{rv} = \nu_{\rm corr}$	500	600	600
(13000–14000 cm^{-1})	J'' odd: $\nu_{rv} = \nu_{\rm corr} - 7.6(3.0) \times 10^{-4}$			
atlas II	J'' even: $\nu_{rv} = \nu_{\rm corr}$	250	600	600
(14000–15800 cm^{-1})	J'' odd: $\nu_{rv} = \nu_{\rm corr} - 7.6(3.0) \times 10^{-4}$			
atlas III	J'' even: $\nu_{rv} = \nu_{\rm corr}$	250	660[1]	450
(14800–20000 cm^{-1})	J'' odd: $\nu_{rv} = \nu_{\rm corr} - 8.2(2.0) \times 10^{-4}$			

[1] Value estimated, see text.

recommendation by [27] about the influence of the hyperfine parameters on the prediction of transition frequencies. The hyperfine shift calculated from the interpolated hyperfine parameters was subtracted, and the resulting three frequencies, which ideally should coincide, were averaged. The uncertainty of the resulting pure rovibrational frequency was estimated from the scatter of these three values, but a lower limit of 0.0001 cm^{-1} $\approx$ 3 MHz was assumed. This procedure relies on the accuracy the authors report [24] and on the experience of the nearly 400 averaged frequencies derived from the atlas, taking into account the signal-to-noise ratios of the saturation spectrum and the marker spectrum.

Further data, but with lower precision, were derived from the iodine atlas by Gerstenkorn and Luc (GL atlas) [1], in order to fill remaining gaps in the list of observations with measurements. This applies especially to the red region from 667 nm to 776 nm, and to the range from 514 nm to 526 nm.

For this purpose the quality of the data of the GL atlas was reexamined with great care. Now, that the hyperfine parameters are known to very good accuracy the profiles can be simulated with better reliability than was possible earlier [34]. The lineshapes of the lines in the atlas are a convolution of overlapping, Doppler broadened hyperfine lines with a rectangular profile due to the finite aperture of the Fourier spectrometer used, and with the instrumental sinc profile.

For the evaluation, the Doppler widths were defined by the temperatures reported for the recording of the different parts of the atlas, and the width of the sinc was taken from [34]. The width of the rectangle was chosen to give best agreement with the widths of the profiles after each step of convolution compared to the values given in [34]. We simulated the line shapes with the line positions of the hyperfine lines calculated from interpolated hyperfine parameters and relative intensities calculated for an electric dipole hyperfine transition.

With this approach, it was possible to determine the shift of the point of maximum intensity of the lines, to which the atlas refers, with respect to the frequency of the pure rovibronic transition. Actually, Gerstenkorn et al. discuss the displacements from the center of gravity of the structure. This differs from the former one by less than 3 MHz, which is negligible within the limits of uncertainty of these spectra. A distinction had to be made between even and odd J'' for the present analysis, as the resulting profiles show different asymmetries, caused by the different numbers, positions and intensities of the components in the hyperfine patterns.

Additionally, the corrected frequencies of selected lines were compared with their corresponding high precision values, and frequency dependent improved calibration formulae were determined. A slight frequency dependence of the differences over the whole range of the atlasses II and III was found, which was already mentioned by Palmer et al. [35], and was corrected for. The final rules and the parameters applied for the different parts of the atlas are listed in Tables 2 and 3. In Table 2 the estimated uncertainties after correction for unblended lines are also given.

Including the NIR data, about 1500 absolute rovibronic frequencies were collected as a basis for the model description. The data field is shown in Figure 2, indicating that the data generally cover both electronic states rather homogeneously. For the ground state, vibrational levels $v'' \leq 17$ are involved, whereas in the upper state v' ranges up to 43. However, the different qualities of the data should be kept in mind. For example for $8 \leq v'' \leq 11$ most data come from the GL atlas, and therefore are less accurate than the other data. This also means that there is no direct connection by high precision measurements from the lower set of vibrational ground state levels $0 \leq v'' \leq 7$ to the higher ones $12 \leq v'' \leq 17$. Generally this results in different levels of precision in the description of parts of the spectra, here especially for the range between 667 nm and 778 nm, and finally gives different

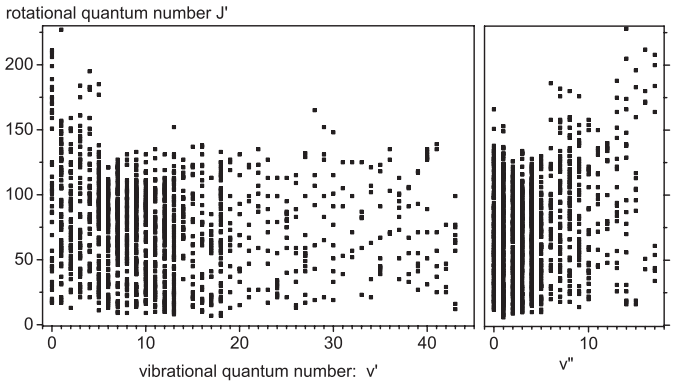

Fig. 2. Input data field for fit: each symbol represents a rovibronic level either in the excited state (left panel) or in the ground state (right panel).

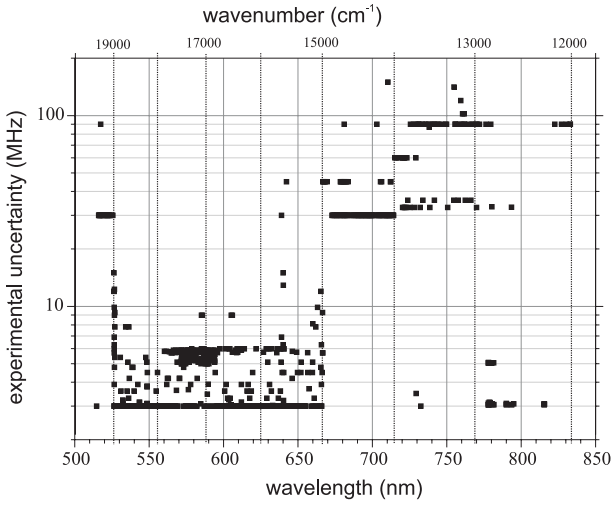

Fig. 3. 1σ uncertainties of the data used for the modelling.

levels of uncertainties for the lines predicted by the model, depending on the bands to which the lines belong. Also included in the data set are the line P(33) of the 6-3 band of the isotopomer $^{129}I^{127}I$, and P(33) 6-3, P(54) and R(69) 8-4, P(110) 10-2, P(69) 12-6, R(113) 14-4 of $^{129}I_2$ [10], They will help to determine correction parameters to the Born-Oppenheimer approximation (see next section). An overview of the absolute uncertainties of the data used in the different spectral ranges is shown in the diagram of Figure 3. Generally the minimum uncertainties were set to 3 MHz, in order to avoid too high weights in the fit for the most precise data (uncertainties down to few kHz), and as we believe that the method used is not capable of describing those data to such a high level of accuracy. In the range from 19000 to 15000 cm^{-1} the precision of the data is generally better than 10 MHz, with only a few exceptions. Additionally there are short intervals in the NIR from our high precision measurements described above, and the precise data at 514 nm [36]. Between these ranges data of the iodine atlas by Gerstenkorn [1] rather bear uncertainties of 30 MHz or slightly higher, according to the last column in Table 2. The complete set of assigned transition frequencies used is provided in the electronic supplement to this paper (see the table in "Online material").

3.2 The physical model applied

The main goal of this paper is to present a model description of the spectroscopic data, which is based on well established theoretical approaches and yields a proper representation of the input data across the whole range with as few parameters as possible. Moreover, it should also be able to interpolate to predict unobserved transitions within that range with a minimal loss of accuracy relative to that of the input data.

An often used approach is the reduction to Dunham parameters [29], which was also applied in Chapter 2 for the narrow range of near infrared data. However, depending on the structure of the data, there is often the problem of strong correlations among the set of parameters of a given state, as well as between the sets of parameters of the two states. This applies especially to correlations between the rotational parameters and the centrifugal distortion constants. One way out of this dilemma can be an iterative approach, where first rough parameter values are determined only for vibration and rotation, neglecting the centrifugal distortions. From these parameters a potential is determined, e.g. by the RKR procedure, and then centrifugal distortion parameters are calculated using the corresponding eigenfunctions of the eigenstates of that potential. The centrifugal parameters are then used as fixed parameters in a further Dunham-parameter fit to determine new vibrational and rotational parameters in the next step of the iteration.

Here we will use as the physical model for the data a very homogeneous approach, which describes each electronic state directly by a model potential, and the energies of the levels are the eigenvalues of the Schrödinger equation solved with these potentials. Several representations of the potentials in such direct potential fits are used in literature, like e.g. the expanded Morse oscillator [37] or modified Lennard-Jones potential [38]. These were developed to describe the whole potential from short to large internuclear separations in a single expression (but sometimes including a switching function accounting for a peculiar representation for the long range part). Other approaches such as the spline interpolated numerical potential of Pashov et al. [39] use their representation only for intermediate nuclear distances, for which data are available, and use reasonable analytical extensions for short and long range extensions.

We will here use potentials in the so-called "X-representation", where the central part supported by data is written as a truncated power series of the form

$$V(R) = \sum_i a_i X^i,\ i = 0, 1, 2, ... \tag{3}$$

with

$$X = \frac{R - R_m}{R + b\ R_m}. \tag{4}$$

The parameters a_i are determined in a fit, R is the nuclear distance and R_m is an arbitrarily chosen expansion center close to the equilibrium nuclear distance of the electronic state. The parameter b allows one to modify the slope at short internuclear distances, and is adjusted once for a best fit of the potential representation (3) to the potential to start with, which in this case was an RKR potential.

This representation was recently used to derive a precise potential for the ground state of the Ca_2 molecule, for which it was also compared with Pashov's approach [40], and was also used successfully for a high precision description of the Na_2 ground state up to the dissociation continuum close to the hyperfine asymptotes [41]. Here we have the opportunity to check whether the principal limits of a potential description are reached already by the very precise data available.

The energy contributions, which are neglected within the Born-Oppenheimer approximation ("Born-Oppenheimer corrections", BOC), must be considered because of the very accurate data. However, they are taken into account only for the excited B state. The BOC contributions to the low levels of the ground state involved here are expected be small, and were therefore neglected in the calculations. However, the parameters derived for the upper state can contain some contribution of the ground state as well.

For the B state the effective Hamiltonian for the radial motion has the form derived by Herman and Ashgarian [42], including adiabatic correction $V_{\rm corr}$ of the potential and nonadiabatic corrections $\alpha(R)$ of the centrifugal energy and $\beta(R)$ of the kinetic energy was used. Here we refer to the more concise form of the effective Hamiltonian as given in [43]

$$\mathbf{H}_{\rm eff} = -\frac{\hbar^2}{2\mu}\frac{\partial}{\partial R}[1+\beta(R)]\frac{\partial}{\partial R} + V(R) + V_{\rm corr}(R) + \frac{\hbar^2[1+\alpha(R)]J(J+1)}{2\mu R^2}. \quad (5)$$

For a homonuclear molecule these corrections depend on the ratio m_e/μ of the electron mass m_e and the reduced mass μ of the molecule. Because only two of these corrections can be determined simultaneously [44,45], we decided to neglect β in our approach, and $\alpha(R)$ becomes the effective nonadiabatic correction, not only the rotational correction. The adiabatic correction $V_{\rm corr}(R)$ can only be determined if data for different isotopic species of the molecule are included. Both $V_{\rm corr}$ and α are functions of the internuclear distance R and are represented also as a truncated power series in X, respectively:

$$\alpha(R) = \frac{\mu_{\rm ref}}{\mu}\ \frac{2R_m}{R+R_m}\sum_i \alpha_i\, X^i,\ i=0,1,2,... \quad (6)$$

$$V_{\rm corr}(R) = \left(1-\frac{\mu_{\rm ref}}{\mu}\right) V_{ad} \quad (7)$$

with

$$V_{ad} = \frac{2R_m}{R+R_m}\sum_i v_i\, X^i,\ i=0,1,2,... \quad (8)$$

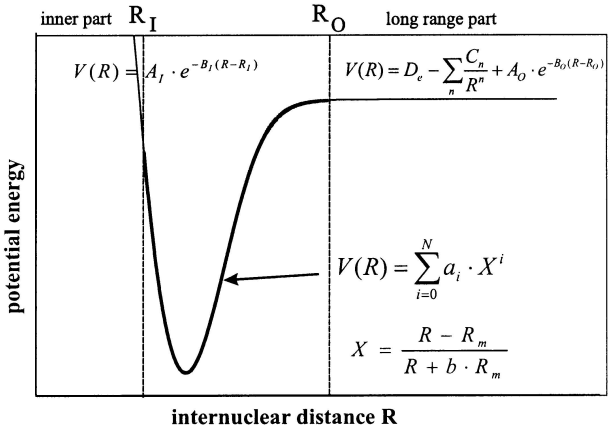

Fig. 4. Construction details of the potentials, for the meaning of the parameters used see text.

with $\mu_{\rm ref}$ being the reduced mass of the selected reference isotope $^{127}I_2$. This ansatz considers the asymptotic behaviour of the corrections in a way proposed recently by Le Roy [46]. $V_{\rm corr} = V_{\rm corr}(\mathrm{B}) - V_{\rm corr}(\mathrm{X})$ asymptotically corresponds to the isotope shift of the atomic transition, which is here $^2P_{1/2}$–$^2P_{3/2}$ of iodine. To our knowledge the isotope shift is not known experimentally, anyway it should be quite small because the transition is only due to a change in the fine structure level. Thus it is justified to set the asymptotic value of $V_{\rm corr}$ to zero. The simplified ansatz turns out to be convenient here, also because no extrapolation to outside the range defined by the input data is intended presently.

In Figure 4 the general construction of the potential form is illustrated. Physically appropriate extrapolation functions are attached outside the range of internuclear distances on which the potential is determined by experimental data. For the inner branch $R < R_I$ an exponential $V(R) = A_I \exp(-B_I(R - R_I))$ is used, where A_I and B_I are adjusted to give a smooth and differentiable connection at R_I after each modification of the central part (heavy line) of the potential. The outer branch $R > R_O$ is extended with functions representing dispersion interactions $V(R) = D_e - \sum_n C_n/R^n + A_O \exp(-B_O(R - R_O))$. The parameters D_e and C_n are taken from literature [47–49]. The parameters of the exponential term are again adjusted to insure smoothness and differentiability at the connection R_O. For both the adiabatic and the nonadiabatic corrections, the representation of equations (6, 7) was used for the total range of R.

During the fit the eigenvalues for the lower and the upper levels are calculated for each optical transition using the Numerov method [50] with the respective potentials, and their difference "cal" is subtracted from measured frequency "obs". The parameters a_i, α_i and v_i are adjusted searching for a minimum of χ^2

$$\chi^2 = \sum_i \left(\frac{obs_i - cal_i}{\Delta obs_i}\right)^2, \quad (9)$$

Δobs_i is the uncertainty of the experimental value. The fitting strategies for this nonlinear problem are provided by the MINUIT program package [51].

3.3 Results

The potential fit is started with an approximation provided by an RKR potential, which is calculated from the Dunham parameters of [25] and transformed to a representation according to equation (3). For different values of b starting from zero in a linear least squares fit of equation (3) to the RKR potential the parameters $a_i, i = 0, ..., N$ for a given number N are determined. While varying b the rms error of those fits is minimized to get the best value for b under these conditions. This value of the parameter b in equation (3) is then kept fixed. The corresponding values of a_i give the starting potential. The parameters α_i and v_i, representing small contributions to the Hamiltonian, were initially set to zero. With these values the nonlinear fit is started. Usually only the parameter set for one chosen electronic state was adjusted, varying step by step more parameters, while keeping the parameters of the other state fixed, and vice versa. After reaching a fairly good fit also the Born-Oppenheimer corrections were released and adjusted. Only parameters that turned out to be significant were kept. Finally all parameters were released and simultaneously fitted.

The excellent quality of the fit is revealed by Figure 5. Here the ratios of the residuals normalized to the experimental uncertainty $(obs - cal)/\Delta obs$ are shown in a histogram, which represents the statistical distribution, i.e. the number of values falling into a certain box of width bw versus the relative distance of the box from zero. The distribution fits well to a Gaussian shape of the functional form $y = y0 + A\exp(-0.5((x - xc)/w)^2)$ with $y0$ and xc set to zero. Thus no systematic shift is contained in the distribution. The full width at half maximum (FWHM) results to 1.0, stating that 66% of the data fall into an interval given by ± 0.5 times the experimental uncertainty around zero. This is of course partly due to giving the data a minimum uncertainty of 3 MHz, while some of them are more precise.

However, there are still some peculiarities in the distribution. In particular, for the 33-0, 34-0, 35-0 bands the differences $obs-cal$ for moderate J'' are systematically negative and the residuals amount up to 5 MHz, in spite of the precise data available there, while lines of high J'' and low J'' of these bands fit quite well. The reason is not known. If it is not a physical effect, an explanation could be the structure of the data set used. In particular, taking the atlas by Kato [24] at the end of its range close to 19000 cm^{-1}, transitions are distributed such that the range of J' systematically increases with the value of v'. So an artificial correlation between the J-dependent and v-dependent parameters could be introduced. Unfortunately, this cannot be avoided presently because no other precise data are available in that region. In this sense the reliability of the fit was improved significantly when the hyperfine lines

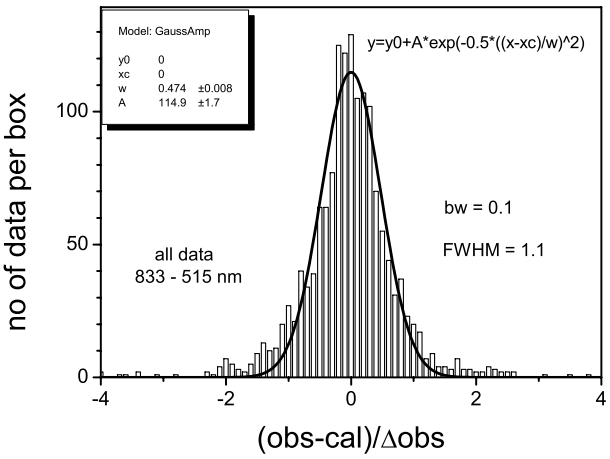

Fig. 5. Histogram of the relative residuals of the fit.

P(42) and R(45) of the 39-2 band near 532 nm [52] could be introduced in the fit.

The potential parameters finally found and the other parameters used for both lower and upper state are given in Table 4. All parameters are given to more than sufficient accuracy, mostly full machine accuracy. It was checked that the data can be reproduced from these numbers to their full accuracy. Because the parameters for upper and lower state are expected to be correlated and the coefficients are not known from this nonlinear fit, individual uncertainties for each parameter are not given. But with the potential the level scheme of each state can be predicted with accuracy similar to that of the the experimental transitions, as discussed in Section 4.

4 General discussion of the results

A very precise and complete set of data known for a molecular optical transition is available for the iodine spectrum under consideration here. The good quality of the fit (Fig. 5) shows the consistency of the data and that the selected model ansatz is adequate. Thus, one can expect a small uncertainty for the prediction of lines using this model. What are reasonable limits of uncertainty for such predictions?

Using the results of the statistics of the residuals of the fit together with Figure 3 for the distribution of the experimental accuracy, the expected uncertainties in the respective spectral ranges can be specified in a simple rule of thumb.

2σ corresponds roughly to the experimental uncertainty, which can be read from Figure 3 as the prevailing uncertainty values. Thus, 92% of the predictions fall into an interval of $\pm$ 3 MHz in the range from 19000 cm^{-1} (526 nm) to 15000 cm^{-1} (667 nm) and from 12880 cm^{-1} (776 nm) to 12270 cm^{-1} (815 nm), because most of the data in the fit have this uncertainty. The lines at 514 nm coinciding with the green Ar+ laser line are fully reproduced within their uncertainty, and the two calibrations at 730 nm ([16]) as well. However, in the remaining range

Table 4. Potential data of upper and lower state and of the BOC functions $\alpha(R)$ and $V_{\rm ad}(R)$ for the reference isotopomer $^{127}I_2$.

parameter	upper state $B0_u^+$	lower state $X^1\Sigma_g^+$
R_m [Å]	3.02669183	2.66638233
b	–0.75	–0.60
a_0 [cm^{-1}]	15769.0678546	0.0
a_1 [cm^{-1}]	$0.888929155287492279 \times 10^1$	$0.947051006049874633 \times 10^1$
a_2 [cm^{-1}]	$0.850235519686038970 \times 10^4$	$0.492602562595701165 \times 10^5$
a_3 [cm^{-1}]	$0.695917336737764890 \times 10^4$	$0.213682631498861410 \times 10^5$
a_4 [cm^{-1}]	$0.994920182775927628 \times 10^3$	$-0.181879788791815008 \times 10^5$
a_5 [cm^{-1}]	$-0.556131449320786032 \times 10^4$	$-0.499045801469034486 \times 10^5$
a_6 [cm^{-1}]	$-0.107555928627667199 \times 10^5$	$-0.702742764701535925 \times 10^5$
a_7 [cm^{-1}]	$-0.169188457283073476 \times 10^5$	$-0.882312608143186953 \times 10^5$
a_8 [cm^{-1}]	$-0.153304207986605579 \times 10^5$	$-0.102331582920833287 \times 10^5$
a_9 [cm^{-1}]	$0.433363227519699431 \times 10^5$	$0.339528118110142939 \times 10^6$
a_{10} [cm^{-1}]	$0.625822290457034105 \times 10^5$	$0.628206506769069820 \times 10^5$
a_{11} [cm^{-1}]	$-0.389266247379213921 \times 10^6$	$-0.717230249674846511 \times 10^7$
a_{12} [cm^{-1}]	$-0.432218520110222744 \times 10^6$	$0.855012363130142097 \times 10^6$
a_{13} [cm^{-1}]	$0.272340536816511489 \times 10^7$	$0.40925020305406115 \times 10^8$
a_{14} [cm^{-1}]	$0.321856089579221839 \times 10^7$	
a_{15} [cm^{-1}]	$-0.127338456382425241 \times 10^8$	
a_{16} [cm^{-1}]	$-0.172753342751943097 \times 10^8$	
a_{17} [cm^{-1}]	$0.425256255365765169 \times 10^8$	
a_{18} [cm^{-1}]	$0.712696682021539360 \times 10^8$	
a_{19} [cm^{-1}]	$-0.913057098990224898 \times 10^8$	
a_{20} [cm^{-1}]	$-0.210868067425342679 \times 10^9$	
a_{21} [cm^{-1}]	$0.926719291015004069 \times 10^8$	
a_{22} [cm^{-1}]	$0.413233196395634711 \times 10^9$	
a_{23} [cm^{-1}]	$0.608534295451399982 \times 10^8$	
a_{24} [cm^{-1}]	$-0.487970270485778809 \times 10^9$	
a_{25} [cm^{-1}]	$-0.305239338118491709 \times 10^9$	
a_{26} [cm^{-1}]	$0.269185593565317631 \times 10^9$	
a_{27} [cm^{-1}]	$0.349461001962127566 \times 10^9$	
a_{28} [cm^{-1}]	$0.277101477602953948 \times 10^8$	
a_{29} [cm^{-1}]	$-0.133371646903035790 \times 10^9$	
a_{30} [cm^{-1}]	$-0.765550455925225466 \times 10^8$	
a_{31} [cm^{-1}]	$-0.136649829213649314 \times 10^8$	
α_0	$-0.257024561963860657 \times 10^{-3}$	
α_1	$0.304354657912661525 \times 10^{-4}$	
α_2	$-0.824779020512065772 \times 10^{-3}$	
α_3	$-0.321720674688543535 \times 10^{-3}$	
α_4	$-0.484148886990049172 \times 10^{-3}$	
v_0 [cm^{-1}]	–0.227614214611850801	
v_1 [cm^{-1}]	$-0.847450483731850923 \times 10^1$	
v_2 [cm^{-1}]	$0.725562196053643760 \times 10^1$	
extension data used		
R_I [Å]	2.64700	2.40000
A_I [cm^{-1}]	0.19603113×10^5	0.45807577×10^4
B_I [Å^{-1}]	0.13702730×10^1	0.90114269×10^1
R_O [Å]	4.90000	3.30000
A_O [cm^{-1}]	0.44452892×10^2	0.10523133×10^4
B_O [Å^{-1}]	0.71764654	0.12830221×10^1
D_e [cm^{-1}]	20150.317 [48]	12547.340 [48]
C_5 [cm^{-1}Å^5]	0.3161×10^6 [49]	-
C_6 [cm^{-1}Å^6]	0.1506×10^7 [49]	0.148×10^7 [47]
C_8 [cm^{-1}Å^8]	0.2480×10^8 [49]	0.386×10^8 [47]
C_{10} [cm^{-1}Å^{10}]	0.0420×10^{10} [49]	0.100×10^9 [47]
range of turning points of potentials [Å]	2.650–4.589	2.427–3.079

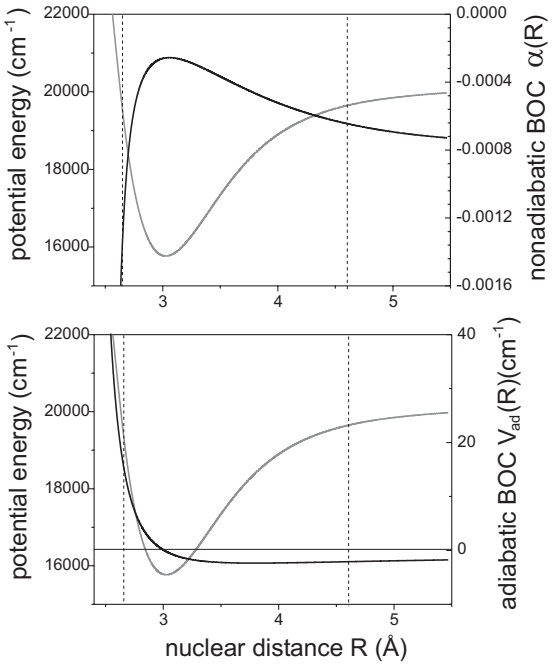

Fig. 6. R-dependent Born-Oppenheimer correction (BOC) parameters (black). Upper panel: effective nonadiabatic correction $\alpha(R)$ for the main isotope $^{127}I_2$; lower panel: adiabatic potential correction $V_{\rm ad}(R)$, both together with the fitted B state potential (grey). The broken vertical lines show the range of turning points covered by data.

between 514 nm and 526 nm one rather has to expect ± 30 MHz as the 2σ interval, and to the red from 667 nm to 776 nm it is partly worse, but 60 MHz will be an upper limit for 2σ. Obviously new data with better accuracy would improve the description significantly. Beyond 776 nm our high precision data are described to better than 1.5 MHz as long as the rotational quantum number J'' is less than about 120, above this range fit residuals increasing with J'' are observed with a maximum of about 7 MHz at $J'' = 238$ in the 0-15 band, despite the inclusion of an effective nonadiabatic BOC by $\alpha(R)$.

The results for the Born-Oppenheimer corrections can in principle help to improve the understanding of the physics of the chemical bond of the iodine molecule in the excited B state. It was verified, that the introduction of the effective adiabatic and nonadiabatic BOC was necessary to get a satisfactory fit. The nonadiabatic term $\alpha(R)$ is determined by the huge manifold in J going up to 238, but the data basis for the other isotopomers, six lines of $^{129}I_2$ and one for the mixed $^{127}I^{129}I$, is still very poor for determining $V_{\rm corr}(R)$. Thus, it is not clear how reliable the corrections, especially their dependence on the internuclear separation, really are.

In Figure 6 the potential energy curve of the B state together with the effective nonadiabatic BOC (upper panel) and the effective adiabatic BOC (lower panel) are shown. Both increase with increasing overlap of the electronic wavefunctions of the two atoms. This is reasonable as one can expect increasing mixing of configurations and therefore deviation from the simple Born-Oppenheimer picture.

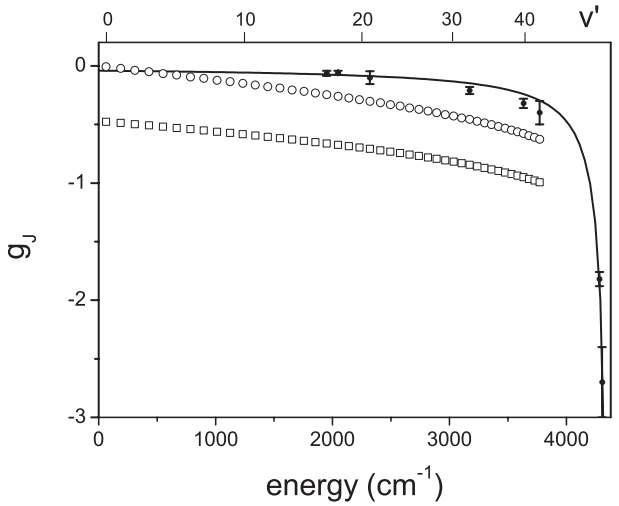

Fig. 7. Molecular g_J-factor as function of the vibrational energy in the excited state. The full line is the vibrational dependence given in [53] and the full circles are the corresponding measurements. The open squares are vibrational averages calculated from the effective nonadiabatic Born-Oppenheimer term α of the present work, the open circles are vibrational averages from a fit with the constraint $\alpha_0 = 0$.

If α were the pure rotational adiabatic correction, its expectation value for level v would be proportional to the molecular g_J factor. The proportionality factor is provided by the ratio of the proton mass m_p and the electron mass m_e [43]:

$$g_J = \frac{m_p}{m_e}\langle v|\alpha(R)|v\rangle. \qquad (10)$$

To check this assumption, vibrational averages of α have been calculated. They are displayed in Figure 7, together with g_J factors determined experimentally by Broyer et al. [53].

The order of magnitude is correct, but the difference between the direct measurements of [53] and the averaged α is large. The experimental values of g_J suggest to set α_0 to very low values. Thus we also tried a fit with the constraint $\alpha_0 = 0$. The final χ^2 is then 870 instead of 830 as before for 1513 observations. This is hardly significant in the statistical sense. The graph of calculated g_J in this case (open circles) is similar in slope compared to that shown in Figure 7, but the offset from zero is nearly completely removed. Obviously the correlation among the parameters is so large, that α_0 can be absorbed in the remaining parameters. In total, the graph of the averaged α is thus much closer to the experimental g_J. But this choice of $\alpha_0 = 0$ is arbitrary and not physically justified. In both cases the calculated values show an increase to higher levels as do the experimental g factors, but with different slope. One might attribute this to the contribution of β (comp. Eq. (5)) to the effective α, but this cannot be decided from the data available.

So despite the large range of rotational quantum numbers in the data set and its high precision α seems to be only poorly determined (see the large difference between

open circles and squares in Fig. 7). The reason is not clear currently.

Thus new experiments enhancing the data basis, especially with respect to the other isotopomers would be very promising for a deeper understanding at this point.

5 Conclusion

A model for a very precise description of a large portion of the visible iodine spectrum is presented. It relies on the simultaneous fit of two potentials to optical transitions. Due to the high precision of the data available it is needed to include the effective rotational correction to the Born-Oppenheimer approximation, and due to the existence of few data on isotopomers ^{127}I^{129}I and ^{129}I$_2$ also an effective adiabatic BOC could be inferred, but more data on these isotopes are desirable for a conclusive statement about the R-dependence of the Born-Oppenheimer corrections.

The resulting model description can be used to predict frequencies of rovibrational transitions of the iodine molecule. Together with the interpolation formulae for the hyperfine parameters the hyperfine structure can be calculated and added. In this way it is possible to predict the hyperfine transition frequencies at a (1σ) level of uncertainty of few MHz, which is useful for calibration purposes of other spectra. Compared to the atlas by Gerstenkorn and Luc [1], the improvement is more than a factor of ten. The potential and the hyperfine structure calculations have been built together in a computer program [54], which can be used conveniently (instead of looking up atlas tables and interpolating graphically there) to calculate the frequencies of iodine transitions and to construct the iodine spectrum in line shape, width and intensity appropriate to the experimental conditions, if Doppler broadened or Doppler reduced. They can be used for calibration of other spectra.

The very informal and efficient help of Harald Schnatz, PTB Braunschweig, who was able to measure promptly frequencies of weak iodine lines at 532 nm, is gratefully acknowledged.

References

1. S. Gerstenkorn, P. Luc, *Atlas du spectre d'absorption de la molecule d'iode*, Laboratoire Aimé Cotton, CNRS II, 91405 Orsay (France), 14 000 cm^{-1}–15 600 cm^{-1} (1978), 15 600 cm^{-1}–17 600 cm^{-1} (1977), 17 500 cm^{-1}–20 000 cm^{-1} (1977), S. Gerstenkorn, J. Verges, J. Chevillard, *Atlas du spectre d'absorption de la molecule d'iode*, Laboratoire Aimé Cotton, CNRS II, 91405 Orsay (France), 11 000 cm^{-1}–14 000 cm^{-1} (1982)
2. A. Morinaga, K. Sugiyama, N. Ito, J. Helmcke, J. Opt. Soc. Am. B **6**, 1656 (1989)
3. A. Arie, R.L. Byer, Opt. Comm. **111**, 253 (1994)
4. S. Kremser, B. Bodermann, H. Knöckel, E. Tiemann, Opt. Comm. **110**, 708 (1994)
5. P. Jungner, M.L. Eickhoff, S.D. Swartz, J. Ye, J.L. Hall, SPIE **2378**, 22 (1995)
6. C.S. Edwards, G.P. Barwood, P. Gill, W.R.C. Rowley, Metrologia **36**, 41 (1999)
7. O. Acef, J.J. Zondy, M. Abed, D.G. Rovera, A.H. Gérard, A. Clairon, Ph. Laurent, Y. Millerioux, P. Juncar, Opt. Comm. **97**, 29 (1993)
8. E. Riis, H.G. Berry, O. Poulsen, S.A. Lee, S.Y. Tang, Phys. Rev. A **33**, 3023 (1986)
9. E. Riis, A.G. Sinclair, O. Poulsen, G.W.F. Drake, W.R.C. Rowley, A.P. Levick, Phys. Rev. A **49**, 207 (1994)
10. T.J. Quinn, Metrologia **40**, 103 (2003)
11. C.J. Sansonetti, J. Opt. Soc. Am. B **14**, 1913 (1997)
12. I. Velchev, R. van Dierendonck, W. Hogervorst, W. Ubachs, J. Mol. Spectr. **187**, 21 (1998)
13. S.C. Xu, R. van Dierendonck, W. Hogervorst, W. Ubachs, J. Mol. Spectrosc. **201**, 256 (2000)
14. B. Bodermann, G, Bönsch, H. Knöckel, A. Nicolaus, E. Tiemann, Metrologia **35**, 105 (1998)
15. B. Bodermann, M. Klug, H. Knöckel, E. Tiemann, T. Trebst, H.R. Telle, Appl. Phys. B **67**, 95 (1998)
16. S.L. Cornish, Y.-W. Liu, I.C. Lane, P.E.G. Baird, G.P. Barwood, P. Taylor, W.R.C. Rowley, J. Opt. Soc. Am. B **17**, 6 (2000)
17. B. Bodermann, M. Klug, U. Winkelhoff, H. Knöckel, E. Tiemann, Eur. Phys. J. D **11**, 213 (2000)
18. H.R. Simonsen, F. Rose, Metrologia **37**, 651 (2000)
19. J. Ye, L. Robertsson, S. Picard, L.-S. Ma, J.L. Hall, IEEE Trans. Instrum. Meas. **48**, 544 (1999)
20. R. Holzwarth, A.Yu. Nevsky, M. Zimmermann, Th. Udem, T.W. Hänsch, J. von Zanthier, H. Walther, J.G. Knight, W.J. Wadsworth, P.St.J. Russell, M.N. Skvortsov, S.N. Bagayev, Appl. Phys. B **73**, 269 (2001)
21. Y. Zhang, J. Ischikawa, F.-L. Hong, Opt. Comm. **200**, 209 (2001)
22. F.-L. Hong, Y. Zhang, J. Ischikawa, A. Onae, H. Matsumoto, Opt. Comm. **212**, 89 (2002)
23. F.-L.Hong, Y. Zhang, J. Ischikawa, A. Onae, H. Matsumoto, J. Opt. Soc. Am B **19**, 946 (2002)
24. H. Kato, *Doppler-Free High Resolution Spectral Atlas of Iodine Molecule* (Japan Society for the Promotion of Science, 2000)
25. S. Gerstenkorn, P. Luc, J. Phys. Fr. **46**, 867 (1985)
26. F. Martin, R. Bacis, S. Churassy, J. Verges, J. Mol. Spectrosc. **116**, 71 (1986)
27. B. Bodermann, H. Knöckel, E. Tiemann, Eur. Phys. J. D **19**, 31 (2002)
28. B. Bodermann, thesis, Hannover (1998)
29. C.H. Townes, A.L. Schawlow, *Microwave Spectroscopy* (Dover Publications, New York, 1975)
30. D. Shiner, J.M. Gilligan, B.M. Cook, W. Lichten, Phys. Rev. A **47**, 4042 (1993)
31. S. Rakowsky, D. Zimmermann, W.E. Ernst, Appl. Phys. B **48**, 463 (1989)
32. H. Rong, S. Grafström, J. Kowalski, G. zu Putlitz, W. Jastrzebski, R. Neumann, Opt. Comm. **100**, 268 (1993)
33. R. Grieser, G. Bönsch, S. Dickopf, G. Huber, R. Klein, P. Merz, A. Nicolaus, H. Schnatz, Z. Phys. A **348**, 147 (1994)
34. S. Gerstenkorn, P. Luc, Rev. Phys. Appl. **14**, 791 (1979)
35. B.A. Palmer, R.A. Keller, Los Alamos Scientific Laboratory, LA-8251-MS Informal Report UC-34a, 1980
36. R.J. Jones, W.-Y. Cheng, K.W. Holman, L. Chen, J.L. Hall, J. Ye, Appl. Phys. B **74**, 597 (2002)

37. J.Y. Seto, Z. Morbi, F. Charron, S.K. Lee, P.F. Bernath, R.J. Le Roy, J. Chem. Phys. **110**, 11756 (1999)
38. J.Y. Seto, R.J. Le Roy, J. Vergès, C. Amiot, J. Chem. Phys. **113**, 3067 (2000)
39. A. Pashov, W. Jastrzebski, P. Kowalczyk, Comp. Phys. Comm. **128**, 622 (2000)
40. O. Allard, A. Pashov, H. Knöckel, E. Tiemann, Phys. Rev. A **66**, 042503 (2002)
41. C. Samuelis, E. Tiesinga, T. Laue, M. Elbs, H. Knöckel, E. Tiemann, Phys. Rev. A **63**, 012710 (2001)
42. R.M. Herman, A. Ashgarian, J. Mol. Spectr. **19**, 305 (1966)
43. E. Tiemann, J.F. Ogilvie, J. Mol. Spectr. **165**, 377 (1994)
44. J.K.G. Watson, J. Mol Spectr. **80**, 411 (1980)
45. J.K.G. Watson, J. Mol. Spectr. **217**, 157 (2003)
46. R.J. Le Roy, Y. Huang, J. Mol. Struct. (Theochem) **591**, 175 (2002)
47. R. Bacis, D. Cerny, F. Martin, J. Mol. Spectr. **118**, 434 (1986)
48. S. Gerstenkorn, P. Luc, R.J. Le Roy, Can. J. Phys. **69**, 1299 (1991)
49. S. Gerstenkorn, P. Luc, C. Amiot, J. Phys. **46**, 355 (1985)
50. J.M. Blatt, J. Comput. Phys. **1**, 382 (1967)
51. F. James, M. Roos, D506 Minuit, Cern library PACKLIB, 1989
52. H. Schnatz, PTB, private communication (2001)
53. M. Broyer, J.-C. Lehmann, J. Vigue, J. Phys. Fr. **36**, 235 (1975)
54. Such program is available under the name "IodineSpec" from TOPTICA Corp., `www.toptica.com`